INSTRUMENTATION

Improved SPECT Quantification Using Compensation for Scattered Photons

Ronald J. Jaszczak, Kim L. Greer, Carey E. Floyd, Jr., C. Craig Harris, and R. Edward Coleman

Duke University Medical Center, Durham, North Carolina

SPECT images are degraded by the inclusion of Compton-scattered photons within the pulse-height window. Phantom and patient studies with Tc-99m were used to evaluate a compensation method that consists of subtracting a fraction of the image reconstructed using events recorded within a secondary pulse-height window (92–125 keV) from that derived from the photopeak pulse-height window (127–153 keV). Images of line sources in air and in a water-filled phantom were stored. The compensated line spread functions (LSFs) were evaluated. In water, the absolute counting rates for the SPECT LSFs were within 10% of the rates measured in air. The phantom consisted of six solid acrylic spheres (diameters 10, 13, 16, 19, 25, 32 mm) placed within a cylindrical (22 cm diam) distribution of Tc-99m. For sphere diameters greater than 25 mm, the measured image contrasts were within 8% of the true uptake ratios. Our results have shown that high-quality, camera-based SPECT systems can reconstruct artifact-free images by making additional use of projection data acquired in a pulse-height window other than that over the primary photopeak. This compensation method results in qualitative and quantitative improvements for the limited source geometries investigated. Further studies are required to optimize this heuristic approach for other source geometries.

J Nucl Med 25: 893–900, 1984

Compton-scattered photons can degrade single photon emission tomographic (SPECT) images, both qualitatively and quantitatively. As a result of the finite energy resolution of the NaI(Tl) detector, events that are singly or even doubly scattered may be detected within the primary-energy window. The effects of scattered radiation have been investigated for conventional planar imaging, positron computed tomography, and SPECT (*1–17*), but an accurate, practical method of compensation has not been developed for SPECT imaging.

A simple approach to compensating for scatter is to use a smaller value for the linear attenuation coefficient, such as 0.12 or 0.13 cm^{-1}, as we and others have shown (*18*). By this expedient one compensates for scatter by undercorrecting for attenuation as it occurs in the medium, under the assumption that a fixed fraction of the attenuated primary photons can be replaced by scattered photons that behave like unattenuated photons. This can produce acceptable results for certain source geometries. For example, because of the acceptance of scattered photons by the photopeak window, the use of 0.12 cm^{-1}, rather than 0.15 cm^{-1}, results in a relatively uniform reconstructed image of a cylindrical source distribution, exhibiting neither decreased nor increased count density towards the central region. However, this method is inadequate for quantification. For example, when a value of 0.12 cm^{-1} is used as the effective attenuation coefficient, the count density measured from a SPECT image of a photon-deficient sphere, 6 cm in diameter and placed near the center of a cylinder, 22 cm diameter by 25 cm long and containing a uniform distribution of Tc-99m, would erroneously indicate that the sphere is "emitting" gamma photons at a rate ~30% of the cylinder's background activity. The erroneous counts are a result of detected scattered photons, since partial-volume effects

Received Mar. 2, 1984; revision accepted Apr. 18, 1984.

For reprints contact: Ronald J. Jaszczak, PhD, P.O. Box 3949, Dept. of Radiology, Duke University Medical Center, Durham, NC 27710.

and finite spatial resolution cannot account for such a flux in the case of a large (6-cm) photon-deficient sphere. Thus, although this method is simple and expeditious and may be reasonable for qualitative SPECT imaging, it can result in large quantitative errors, as in the above example.

A second approach is to use the first method to produce the SPECT image, but to compensate region-of-interest data obtained from that image by using an estimated average value for the scatter fraction, SF_{avg}. We have shown (*18*) that such an approach can indeed improve the accuracy of specific SPECT measurements. The study showed that if Q_s is the radionuclide concentration within an acrylic hollow sphere, placed within a cylinder containing a uniform source distribution having a concentration Q_b, the ratio Q_s/Q_b can be more accurately estimated using the following equation:

$$Q_s/Q_b = (C_{image}/CF_{avg})(1 + SF_{avg}) + 1, \quad (1)$$

where C_{image} is the SPECT-measured contrast for the sphere's image, CF_{avg} is the contrast loss factor due to the system's finite spatial resolution, and SF_{avg} is the estimated value for the average scatter fraction in the reconstructed SPECT image. In that investigation (*18*) a value of 0.4 was assumed for SF_{avg}. For the measurement of concentration ratios, SF_{avg} need be only approximately known. For example, the value of 0.4 may be in error, but changing SF_{avg} to 0.3 (a 25% decrease) results in only a 7% decrease in the SPECT-measured concentration ratio. This second method for scatter compensation assumes either that the scatter fraction does not vary within the SPECT sectional images, or alternatively that large changes in the assumed value for SF_{avg} result only in small errors in the parameter that is being quantified. Although these assumptions may be useful for the determination of concentration ratios within a cylindrical source, the equation cannot be used easily to obtain absolute concentrations within a specific region of interest, since the structured nature of the scatter image would affect these measurements.

Because of these deficiences, we have developed a new approach to scatter compensation. A first objective of this research was to determine whether scattered photons detected within an energy window located below the primary energy could produce artifact-free reconstructed images. It has recently been reported (*19*) that it may not be possible to reconstruct artifact-free SPECT images using an energy window located on the Compton portion of the energy spectrum, since the projection data are inherently inconsistent. Furthermore, it is possible that the flood-compensation algorithm and/or the intrinsic response of the scintillation camera could be inadequate. Thus, attainment of this first objective is a necessary, but not sufficient, prerequisite for the successful implementation of the proposed scatter-compensation procedure. The second objective was to evaluate qualitatively and quantitatively a compensation procedure whereby a fraction, k, of the image reconstructed using events recorded within the lower secondary energy window, is subtracted from the image reconstructed using events recorded within the primary photopeak window. The fraction k has been determined heuristically for our SPECT acquisition system and reconstruction algorithm. A procedure to compensate for scattered photons in reconstructed SPECT images is described in the following section. The method is based on the assumption that the scatter image reconstructed from events collected within the scatter window is a reasonably close approximation to the true scatter component of the image reconstructed from the photopeak window. Technetium-99m line source, phantom, and patient data are presented to validate the compensation procedure.

MATERIALS AND METHODS

Data acquisition and reconstruction. The SPECT system (*20*) consisted of dual, large-field-of-view scintillation cameras*, mounted within a rotatable gantry and interfaced to a 32-bit minicomputer having one megabyte of memory. SPECT projection data were acquired with continuous rotational motion of the gantry composed of 180 angular samples framed into 2° intervals. The linear sampling interval was 3.2 mm. The time was 26 min for a complete 360° revolution of each detector. The pixel slice thickness along the axis of rotation was typically 12.8 mm, although for some images two adjacent slices were summed. Data were acquired using high- or ultrahigh-resolution, parallel-hole collimators. The reconstructed spatial resolutions on axis, using a 15-cm radius of revolution were equal to 10.5 ± 0.5 mm for the high-resolution and 9.0 ± 0.5 mm for the ultrahigh-resolution collimators. Projection data were acquired using two pulse-height windows. A window centered at 140 keV (127 to 153 keV) was used for the primary photopeak events. A secondary window bracketing 92 to 125 keV collected scattered events. This is the same pulse-height window used to generate the body contour used by the first-order attenuation-compensation algorithm (*20,21*).

Images were reconstructed into a 128 × 128 matrix using a filtered backprojection algorithm. Generalized Hanning windows (*18*) were used, having cutoff frequencies equal to 1.6 cycles/cm for the photopeak events, and 0.4 to 0.8 cycles/cm for the events recorded in the secondary pulse-height window. The latter values for the cutoff frequencies were specifically chosen for the scatter-window data to minimize degradation of the reconstructed scatter image. A value of 0.15 cm^{-1} was used as the attenuation coefficient for the first-order compensation procedure. Projection data were compensated for nonuniform detector response using a multiplicative procedure. The correction matrix was

generated from planar images (45 million counts) of a Tc-99m sheet source acquired with the primary photopeak window. Flood images acquired with the secondary window were compared with photopeak flood images. The flood nonuniformities observed in the two images were similar, and no artifacts were generated in the reconstructed images using the lower pulse-height window as a result of the flood compensation algorithm.

Phantom and patient data. Two Tc-99m line sources (5 mm i.d. by 5 cm long) were imaged in air and in a water-filled cylindrical phantom† 22 cm in diameter. One line source was placed in the axis of rotation and imaged. This source was then removed and the second source was placed 8 cm from and parallel to the axis of rotation, and imaged.

These data were qualitatively and quantitatively evaluated to determine the factor k used by the compensation procedure. A source with relatively large diameter (5 mm) was used to obtain adequate count densities within the shoulders of the line spread function.

A plastic sphere (6 cm diam), filled with nonradioactive water was placed within the cylindrical phantom (22 cm diam), which contained a uniform distribution of Tc-99m, and an image was made. The center of the sphere was located 2.5 cm from the axis of the cylinder. This large-diameter, count-deficient sphere was chosen to minimize the effects of finite spatial resolution on the absolute count density within the reconstructed image of the sphere.

To evaluate the effect of the compensation method on the SPECT imaging of smaller photon-deficient defects, six solid methylmethacrylate spheres (diameters 9.5, 12.7, 15.9, 19.1, 25.4, and 31.8 mm) were placed within the cylindrical phantom†, and imaged. Counting rates within regions of interest (ROIs) were measured to determine image contrasts and signal-to-noise (S/N) ratios. A sphere's image contrast is defined as the difference between the count density (counts/pixel) in a small ROI within the image of the sphere and the count density in an ROI for the surrounding background, all divided by the background count density. We define the S/N ratio as the net signal (count density in a small ROI within the image of the sphere, minus the background) divided by the standard deviation, of the count density of the background (i.e., the noise level). The ROIs for the spheres were centered within the images of the spheres and ranged from 2 by 2 pixels for the smaller spheres to 5 by 5 pixels for the larger. An average of five ROIs located between the images of the spheres provided the background count density and the noise level.

Compensation procedure. A fraction, k, of the image $f_2(x,y)$ reconstructed using events recorded in the lower window is subtracted from the image $f_1(x,y)$ reconstructed using events recorded in the photopeak pulse-height window, to produce the compensated image f(x,y):

$$f(x,y) = f_1(x,y) - k \cdot f_2(x,y) \quad (2)$$

Two approaches were used to determine the value of k. The first consisted of quantitatively comparing the images of the line source imaged in air using planar imaging, and in a water-filled cylinder using SPECT. The situation in air was taken to approximate the ideal nonscatter geometry. The factor k was varied and—using appropriately placed ROIs (as described below)—the integral of the counts in the compensated SPECT image of the line source in water was compared with the integral of the counts in the planar image of the line source in air. Since the SPECT image of a line source placed parallel to the axis of rotation appears in the reconstructed SPECT image as a "point" structure, the integral of the counts within the SPECT sectional image is obtained by using an ROI that encompasses the entire image (i.e., 128 by 128 pixels for our particular reconstruction algorithm). Since the planar image of the line source appears as a "line" structure, the planar counting rate is obtained by summing the counts under a profile drawn through the planar image of the line source in air. That profile was 128 pixels long and had a width equal to the pixel slice thickness that was used for the SPECT acquisition of the projection data. Furthermore, the profile was located along the planar image of the line source at a position corresponding to that acquisition.

SPECT images of the line source in water and in air, and placed both on-axis and off-axis, were evaluated. The shapes of the profiles of the line sources for values below 0.05 of the peak height were compared. Finally, profiles through the compensated images of the 6-cm water-filled spheres were also evaluated, since an appropriate compensation should result in a mean counting rate of zero within the image of the sphere. This heuristic approach resulted in a value of ~0.5 for the factor k. Using this value the counting rates of the compensated images of the line source in water were within 10% of the count rates of the images of the line source in air.

The second approach in determining the value of k consisted of a Monte Carlo simulation of the SPECT system (*11*). Unlike the experimental devices, the computer simulation is able to distinguish independently between scattered and nonscattered events. Thus the true number of scattered events recorded within the photopeak may be determined. Using the appropriate pulse-height windows and a value of 12% for the energy resolution of the SPECT system, the Monte Carlo program was used to simulate the line source placed within the water-filled cylinder. This simulation resulted in a value of 0.57 for the parameter k. The results presented in the next section were obtained using the experimentally determined value 0.5.

RESULTS

Tc-99m line sources. Profiles drawn through the SPECT images of the line source are presented in Figs.

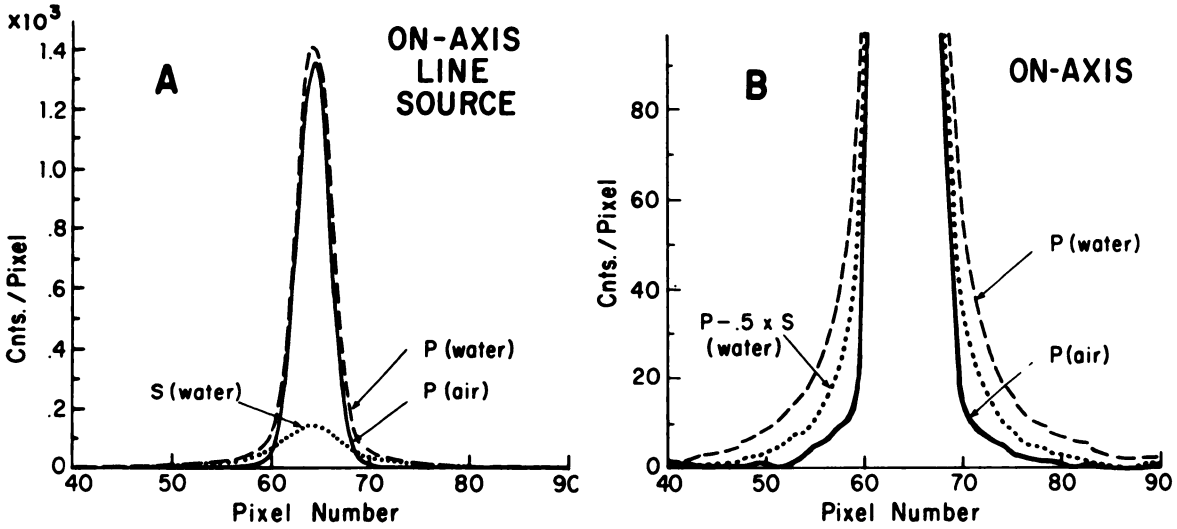

FIG. 1. Count-density histograms drawn through reconstructed SPECT data for on-axis Tc-99m line source (5 mm i.d.) At left are full histograms of images obtained using photopeak (P) and scatter (S) pulse-height windows. Right: histograms through photopeak images of source in air and in water-filled cylinder, together with histogram through compensated image (P − 0.5S). Ordinate has been expanded to emphasize shoulder regions of histograms.

1 and 2. The SPECT image, of course, suggests a "point" structure. The on-axis data for the line source imaged in air and in the water-filled phantom are shown in Fig. 1. In Fig. 1B the ordinate scale has been expanded to emphasize the shapes of the profiles below the level of FWTM. A linear scale has been used to preserve negative data. The original and compensated profiles can be compared with the profile obtained by imaging the line source in air. These results indicate that the shape of the line spread function has been improved by the compensation procedure.

For the off-axis line source data (Fig. 2), two orthogonal profiles were used. A radial profile (Fig. 2A) was drawn parallel to a line passing through the points corresponding to the axis of rotation and the centroid of the image of the line source. A tangential profile (Fig. 2B) was drawn perpendicular to the first profile (i.e., tangent to a circle whose center is at the point corresponding to the axis of rotation and whose circumference passes through the image of the line source). Profiles drawn through the compensated images (P − 0.5 × S) of the line source in water agree closely with the profiles obtained by imaging the line source in air [P(air)]. In Figs. 1 and 2 the lines have been drawn through the measured values.

Table 1 presents the absolute counting rates obtained using the ROIs described in the previous section and measured from the SPECT and planar images of the line sources. These data have been corrected for radionuclide decay, and the SPECT images were attenuation-com-

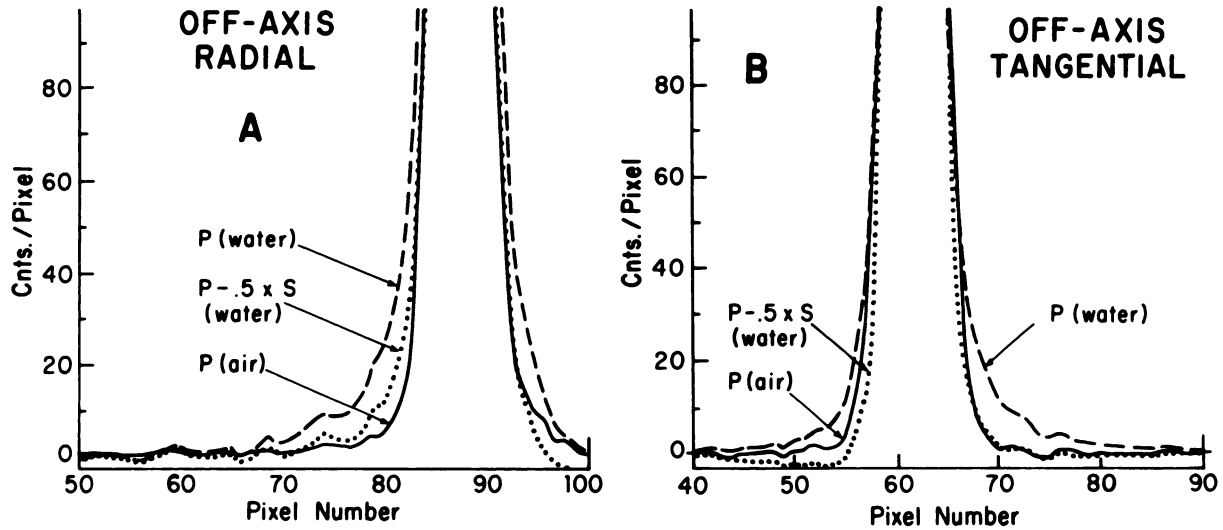

FIG. 2. Radial and tangential histograms drawn through reconstructed SPECT values of off-axis line source. Ordinate has been expanded to emphasize shoulder regions in histograms.

TABLE 1. SPECT COUNTING RATES

Source location	Photopeak image* (kcounts/sec)	Compensated image* (kcounts/sec)	True count rate† (kcounts/sec)
on-axis	8.37	6.60	6.00
off-axis	7.53	4.28	4.49

* Measured from SPECT images of line sources placed within water-filled cylinder (22 cm diam) using large ROI (128 by 128 pixels)

† Measured from planar images of line sources scanned in air using ROI corresponding to location of SPECT projection data (i.e., equal to 128 by pixel slice thickness).

pensated (*20,21*) using a value of 0.15 cm^{-1} for the attenuation coefficient. For the on-axis data the original photopeak counting rate was 40% larger than the counting rate in air. After compensation, the counting rate was 10% larger than the planar counting rate in air. The data are consistent with the profile data, since the compensated values were slightly larger in the shoulders of the profiles than in SPECT images of the line source in air (Fig. 1B).

The original photopeak counting rate for the off-axis line source data was 68% larger than the planar counting rate in air, whereas for the compensated image the counting rate was only 5% less than the planar counting rate. Note that the off-axis line source contained less total activity than the on-axis line source. Again, the data presented in Table 1 for the off-axis location are consistent with the profiles presented in Fig. 2B.

Extended-source distribution. SPECT images of the solid methylmethacrylate sphere (diam. 6 cm) are presented in Fig. 3. The photopeak data contained 3 million events within the 25.6-mm-thick slice shown, whereas the scatter image contained approximately 2 million events. The profile drawn through the original photopeak data indicates a nonzero count density within the image

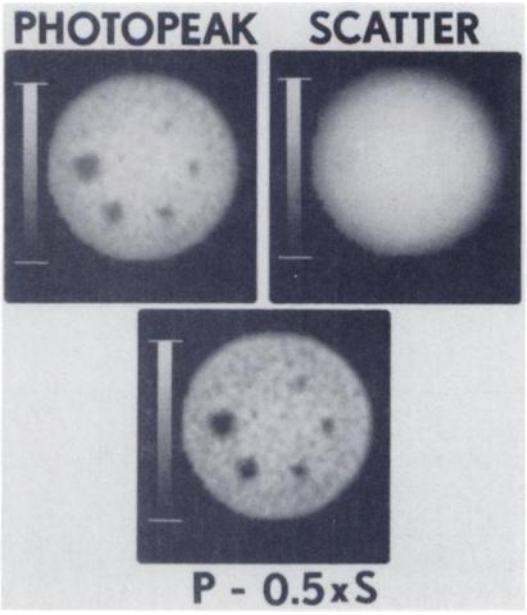

FIG. 4. SPECT images of 6 photon-deficient spheres ranging from 13 to 32 mm in diam, placed in water-filled cylinder† containing uniform distribution of Tc-99m.

of the sphere. The profile drawn through the compensated image (P − 0.5 × S) indicates a nearly perfect compensation within the image of the photon-deficient sphere.

Figure 4 shows images of the set of six photon-deficient spheres placed within the water-filled cylindrical phantom containing a uniform distribution of Tc-99m. The pixel-slice thickness is equal to 12.8 mm. The photopeak image contains 5 million events and the scatter image 3.8 million. Clearly there is increased contrast in the compensated images of the spheres. Table 2 presents the quantitative results for the larger-diameter sphere (6 cm, Fig. 3) and the smaller ones (Fig. 4). The image contrasts for the smaller spheres were increased by a factor of two, and the S/N ratios in the compensated image are comparable to those measured in the photopeak image. For the larger-diameter spheres the image contrasts (i.e., the signal-to-background ratio) very

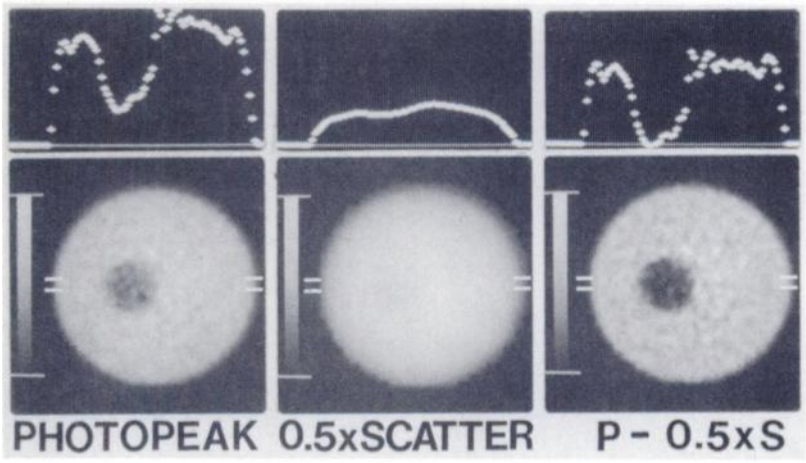

FIG. 3. SPECT images and histograms of photon-deficient sphere (6 cm diam) placed within water-filled cylinder (22 cm diam) containing uniform distribution of Tc-99m.

TABLE 2. IMAGE CONTRASTS, C_{image}, AND SIGNAL-TO-NOISE RATIOS, S/N

Sphere diameter (mm)	Photopeak image		Compensated image	
	C_{image}	S/N	C_{image}	S/N
60	−0.68	5.2	−1.00	5.3
32	−0.66	12.0	−0.98	11.0
25	−0.61	11.0	−0.92	10.0
19	−0.56	10.0	−0.88	10.0
16	−0.34	6.2	−0.58	6.5
13	−0.21	3.0	−0.53	4.4

nearly equaled the true uptake ratio or object contrast (i.e., the difference between the concentrations within the sphere and the cylinder, divided by the cylinder concentration). For these photon-deficient spheres, the uptake ratio is −1.0. Thus for spheres larger greater than 2.5 cm in diameter the compensated SPECT images directly result in values within 8% of the true radionuclide concentrations. The values for the smaller spheres are degraded as a result of the finite spatial resolution (partial-volume effects) of the SPECT system.

In Table 2, the values presented for the 6-cm sphere were measured using a pixel-slice thickness of 12.8 mm. The photopeak image contained 1.6 million events, whereas the scatter image contained 1 million. The percent standard deviations (% s.d.) of the mean background count densities for the photopeak and the compensated images of the 6-cm image were 13% and 20%, respectively. The corresponding values for the photopeak and compensated images of the six spheres were 5% and 8%. Although the absolute noise level is increased in the compensated images, the S/N ratio is comparable to that in the original data.

SPECT transaxial images of a liver/spleen scintigram of a patient with a small (~1 − 2 cm) posterior lesion are presented in Fig. 5. The reconstructed image of events recorded within the scatter window indicates that although high spatial-frequency components are absent, the scatter image cannot be represented by a simple uniform background distribution. The contours of the liver and spleen are clearly delineated. The photopeak and scatter images contain 1.6 and 1.2 million events respectively.

DISCUSSION

The procedure of subtracting a normalized background is similar to standard background-correction techniques used in the quantitative analysis of several experimental procedures. The availability of high-quality, stable scintillation cameras has facilitated the SPECT acquisition and reconstruction of events recorded in pulse-height windows other than that for the primary photopeak window. Since a SPECT image is reconstructed using projection data acquired over a 360° angular range, a moderation, or averaging, of depth-dependent responses results during the backprojection process. This averaging has been observed for depth-related collimation and attenuation effects. It is reasonable to expect a similar averaging to occur for scattered photons. Thus it has been possible to determine a value for the factor k that is not strongly dependent on the location of an emitting source within the scattering medium. In general it may not be possible to determine such a value by operating directly on the projection data instead of the reconstructed images.

The results indicate that the first-order technique can be used to compensate for SPECT-image degradation resulting from the inclusion of Compton-scattered photons within the primary pulse-height window. SPECT images are improved both qualitatively and

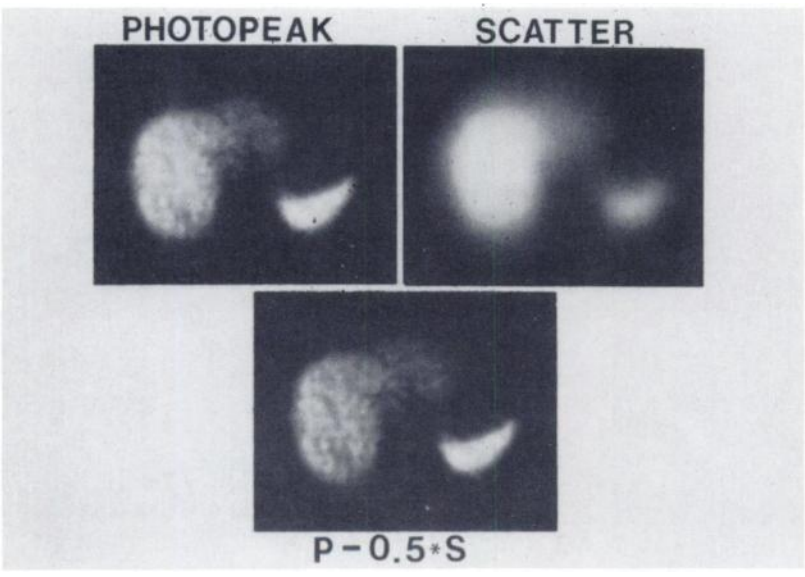

FIG. 5. Liver/spleen SPECT images of patient with small (1–2 cm) posterior filling defect in liver. Patient was scanned for 26 min after injection of 4 mCi of Tc-99m sulfur colloid.

quantitatively by increasing the absolute values of image contrasts, while S/N ratios remain approximately equal to those measured in the original images. The images are qualitatively improved because the image contrasts for small lesions are increased to levels above the visual threshold of the observer, and also because the edges of the large lesions are clearer. More importantly, SPECT data are quantitatively improved because the SPECT-measured values for image contrasts in large lesions may be equated directly to the lesions' uptake ratios. For big enough sources (>2 cm), it should be possible to measure absolute concentrations directly from the SPECT count rates. However, for small lesions (<~2 cm) the effects of finite spatial resolution still degrade SPECT quantification; for these, compensation procedures, such as the use of computed contrast factors (*18*) or recovery coefficients (*22*), must be used to obtain more accurate results. Alternatively, SPECT systems with improved spatial resolution would need to be developed, without loss of sensitivity.

The results presented in Fig. 5 indicate that the scatter image is not completely unstructured. Hence, it is not wholly appropriate to compensate for scatter by assuming a single average value for the scatter fraction (*18*), although this technique has been shown to improve measurements of concentration ratios for spheres placed within a cylindrical phantom. Furthermore, windowing or using other contrast-enhancement techniques (such as a uniform background subtraction) would not be expected to produce quantitative results as accurate as those obtained with the procedure presented here.

One might argue that the scatter in the photopeak has some higher spatial-frequency components compared with the scatter in the lower window because the former contains more narrow-angle scatter, but our Monte Carlo simulations indicate that the spatial frequencies are similar in the two windows.

Several factors can be varied using the scatter-subtraction method. Although the simple heuristic approach presented has produced accurate results for a range of source distributions (both line sources and extended sources), further investigations will be needed to optimize this procedure for other source geometries, as in the case of nonuniform attenuation. Alternatively, it may be possible to compensate for scatter by deconvolving the scatter response from the photopeak image. This appears to be somewhat analogous to the deconvolution and integral transformation procedures that have been proposed (*13,15,23,24*) for both conventional imaging and ECT. We are currently using Monte Carlo simulations of the SPECT imaging system in order to evaluate these approaches.

Our results show that high-quality camera-based SPECT systems can reconstruct low-artifact images using projection data acquired in a pulse-height window other than that covering the primary photopeak. The information contained in photons with energies outside the photopeak window can thus be utilized to enhance SPECT image quality further. Ideally one would want to make use of every gamma photon that interacts with the detector. An approach to use the information obtained from events outside the photopeak has been proposed for conventional imaging by Beck (*2,4*). It is anticipated that as computational capability improves through the increased application of array processors, more-powerful host computers, and larger storage devices, this and other approaches to the problems of scattered photons and finite spatial resolution will be implemented, resulting in further improvements in SPECT quantitative imaging.

FOOTNOTES

* ZLC-37TM, Siemens Gammasonics, Inc., 2000 Nuclear Drive, Des Plaines, IL 60018

† Model 5000, Data Spectrum Corp., 2307 Honeysuckle Road, Chapel Hill, NC 27514.

ACKNOWLEDGMENTS

The authors thank Rainer Haerten and William White of Siemens Gammasonics, Inc., for their support and encouragement. This investigation was supported by PHS Grant Number CA33541 awarded by the National Cancer Institute, DHHS.

REFERENCES

1. BECK RN, SCHUH MW, COHEN TD, et al: Effects of scattered radiation on scintillation detector response. In *Medical Radioisotope Scintigraphy I.* (IAEA: Vienna, 1969), pp 595-616
2. BECK RN, ZIMMER LT, CHARLESTON DB, et al: Aspects of imaging and counting in nuclear medicine using scintillation and semiconductor detectors. *IEEE Trans Nucl Sci* NS-19 (3):173-178, 1972
3. JOHNSTON RE, BRILL AB: Inherent problems in the quantitation of isotope scan data. In *Medical Radioisotope Scintigraphy I* (IAEA: Vienna, 1969) pp 617-631
4. BECK RN, ZIMMER LT, CHARLESTON DB, et al: Advances in fundamental aspects of imaging systems and techniques. In *Medical Radioisotope Scintigraphy I.* (IAEA: Vienna, 1973) pp 3-45
5. BLOCH P, SANDERS T: Reduction of the effects of scattered radiation on a sodium iodide imaging system. *J Nucl Med* 14:67-72, 1972
6. DRESSER MM, KNOLL GF: Results of scattering in radioisotope imaging. *IEEE Trans Nucl Sci* NS-20:266-272, 1973
7. EHRHARDT JC, OBERLEY LW, LENSINK SC: Effect of a scattering medium on gamma-ray imaging. *J Nucl Med* 15:943-948, 1973
8. WAGGETT DJ, WILSON BC: Improvement of scanner performance by subtraction of Compton scattering using multiple energy windows. *Br J Radiol* 51:1004-1010, 1978
9. PANG SC, GENNA S: The effect of Compton scattered photons on emission computerized transaxial tomography. *IEEE Trans Nucl Sci* NS-26:2772-2774, 1979
10. EGBERT SD, MAY RS: An integral-transport method for Compton-scatter correction in emission computed tomogra-

phy. *IEEE Trans Nucl Sci* NS-27:543-547, 1980
11. BECK JW, JASZCZAK RJ, COLEMAN RE, et al: Analysis of SPECT including scatter and attenuation using sophisticated Monte Carlo modeling methods. *IEEE Trans Nucl Sci* NS-29:506-511, 1982
12. KING PH: Noise identification and removal in positron imaging systems. *IEEE Trans Nucl Sci* NS-28:148-151, 1981
13. BERGSTRÖM M, ERIKSSON L, BOHM C, et al: Correction for scattered radiation in a ring detector positron camera by integral transformation of the projections. *J Comput Assist Tomog* 7:42-50, 1983
14. LOGAN J, BERNSTEIN HJ: A Monte Carlo simulation of Compton scattering in positron emission tomography. *J Comput Assist Tomogr* 7:316-320, 1983
15. AXELSSON B, MSAKI P, ISRAELSSON A: Subtraction of Compton-scattered photons in single-photon emission computerized tomography. *J Nucl Med* 25:490-494, 1984
16. FLOYD CE, JASZCZAK RJ, HARRIS CC, et al: Energy and spatial distribution of multiple order Compton scatter in SPECT: A Monte Carlo investigation. *Phys Med Biol:* in press
17. JASZCZAK RJ, COLEMAN RE, GREER KL: The subtraction of scattered events from SPECT photopeak events. *J Nucl Med* 24:P82, 1983
18. JASZCZAK RJ, COLEMAN RE, WHITEHEAD FR: Physical factors affecting quantitative measurements using camera-based single photon emission computed tomography (SPECT). *IEEE Trans Nucl Sci* NS-28:69-80, 1981
19. GULLBERG GT, MALKO JA, EISNER RL: Boundary determination methods for attenuation correction in single photon emission computed tomography. In *Emission Computed Tomography: Current Trends.* Esser, P, ed. (The Society of Nuclear Medicine, New York, 1983) pp 33-53
20. JASZCZAK RJ, CHANG L-T, STEIN NA, et al: Whole-body single-photon emission computed tomography using dual, large-field-of-view scintillation cameras. *Phys Med Biol* 24:1123-1143, 1979
21. CHANG L-T: A method for attenuation correction in radionuclide computed tomography. *IEEE Trans Nucl Sci* NS-25:638-643, 1978
22. HOFFMAN EJ, HUANG SC, PHELPS ME: Quantitation in positron emission computed tomography: 1. Effect of object size. *J Comput Assist Tomogr* 3:299-308, 1979
23. KING MA, DOHERTY PW, SCHWINGER RB, et al: Fast count-dependent digital filtering of nuclear medicine images: Concise communication. *J Nucl Med* 24:1039-1045, 1983
24. METZ CE, BECK RN: Quantitative effects of stationary linear imaging processing on noise and resolution of structure in radionuclide image. *J Nucl Med* 15:164-170, 1974